Philosophical Magazine
Vol. ??, No. ?, Month?? 2008, 1–18

Taylor & Francis
Taylor & Francis Group

Unusual Quasiparticle Renormalizations from Angle Resolved Photoemission on USb_2

Xiaodong Yang[a], P.S. Riseborough[a]*, T. Durakiewicz[b], C.G. Olson[c], J.J. Joyce[b], E. Bauer[b], J.L. Sarrao[b], D.P. Moore[b], K.S. Graham[b], S. Elgazaar[d], P. Oppeneer[d], E. Guziewicz[e] and M.T. Butterfield[f]

[a]*Department of Physics, Temple University, Philadelphia, Pennsylvania 19122, USA;* [b]*Los Alamos National Laboratory, Los Alamos, New Mexico 87545, USA;* [c]*Ames Laboratory, Iowa State University, Ames, Iowa 50011, USA;* [d]*Department of Physics, Uppsala University, Box 530, Sweden;* [e]*Institute of Physics, Polish Academy of Sciences, Warsaw, Poland;* [f]*Lawrence Livermore National Laboratory, Livermore, California 94550, USA*

(*Received 3 October 2008; final version received 15 November 2008*)

Angle-resolved photoemission experiments have been performed on USb_2, and very narrow quasiparticle peaks have been observed in a band which local spin-density approximation (LSDA) predicts to osculate the Fermi energy. The observed band is found to be depressed by 17 meV below the Fermi energy. Furthermore, the inferred quasiparticle dispersion relation for this band exhibits a kink at an energy of about 23 meV below the Fermi energy. The kink is not found in LSDA calculations and, therefore, is attributable to a change in the quasiparticle mass renormalization by a factor of approximately 2. The existence of a kink in the quasiparticle dispersion relation of a band which does not cross the Fermi energy is unprecedented. The kink in the quasiparticle dispersion relation is attributed to the effect of the interband self-energy involving transitions from the osculating band into a band that does cross the Fermi energy.

Keywords: quasiparticles; mass enhancements; electron–phonon interaction; angle resolved photoemission; USb_2

1. Introduction

The electronic dispersion relations of materials which are subjected to large quasiparticle mass enhancements are expected to exhibit kinks in the vicinity of the Fermi energy. These kinks are produced by a rapid cross-over in the quasiparticle masses from their enhanced values at low excitation energies to their unenhanced values at higher excitation energies. This cross-over typically occurs at an energy which is characteristic of the boson-like fluctuations that are responsible for the mass renormalizations [1–7], although recently it has been suggested that kinks can be produced solely by electronic correlations [8]. Kinks in the dispersion relations have been found to be universal features of high-temperature superconductors [9], as has been observed in a number of angle-resolved photoemission experiments [10–12]. The observation of the kinks in superconducting oxides has been aided by the quasi-two-dimensional nature of the materials and the relatively high

*Corresponding author. Email: prisebor@temple.edu

ISSN 1478–6435 print/ISSN 1478–6443 online

DOI: 10.1080/14786430802629501
http://www.informaworld.com

energy scales of the kinks. Uranium compounds, such as UPt_3, have been shown to exhibit large mass renormalizations via measurements in the linear-T term in the electronic specific heat [13]. The quasiparticle mass renormalizations have been confirmed by measurements of the de Haas–van Alphen oscillations [14–16] and via optical absorption measurements of the Drude peak [17]. Although uranium compounds do exhibit large quasiparticle mass enhancements, kinks in the quasiparticle dispersion relations have not been previously seen in uranium compounds since the quasiparticle weights are probably too small. The coefficient of the linear T term in the electronic specific heat of USb_2 [18] is $25\,mJ\,K^{-2}\,mol^{-1}$ which is only moderately enhanced, when compared with heavy-fermion compounds. USb_2 is known to be an antiferromagnet, with a transition temperature of $T_N = 203\,K$ and has relatively large ordered magnetic moments of 1.88 μ_B [19–21]. The moments, which are located on the uranium ions, are aligned either parallel or antiparallel to the c-axis. The Fermi surface has been investigated by de Haas–van Alphen measurements [22] which indicate that the material may have a quasi-two-dimensional character [23–25]. The de Haas–van Alphen measurements also revealed that the 5f bands are split by the antiferromagnetic ordering and yielded quasiparticle masses which are of the order of 1.84–6.0 free electron masses. Due to the quasi-two-dimensional nature of the material, the observed magnitudes of the effective masses and the availability of high-quality single crystals, USb_2 is very suitable for studying the dispersion of the quasiparticle renormalizations in its 5f bands. Therefore, we have examined the electronic dispersion relations in USb_2 via angle-resolved photoemission (ARPES) measurements and have compared these with electronic structure calculations [26].

The electronic structure calculations were performed using the full potential local orbital method [27] adopting the local spin-density approximation (LSDA). In fully relativistic, full-potential calculations, the f-electrons were treated as itinerant and included in the set of valence states. The antiferromagnetic superstructure of USb_2 was assumed in the calculations, and the experimental lattice parameters $a = 4.27\,Å$ and $c = 8.748\,Å$ were adopted. The following basis sets were assumed for U and Sb: 6s6p6d;7s7p and 5f; and 4s4p4d;5s5p, respectively. The Perdew–Wang parameterization [28] of the LSDA exchange and correlation functional was adopted in our calculations. In order to test our LSDA calculation, the optimized theoretical volume (given by the minimum of the total energy) was calculated and found to be 1.2% smaller than the experimental volume. The calculations indicate that USb_2 is a compensated metallic antiferromagnet, in which there are bands with 5f character near the Fermi energy. The electronic dispersion relations as calculated by LSDA are shown in Figure(1). It is seen that the 5f electronic bands have a quasi-two-dimensional character, presumably due to the presence of uranium planes in the structure.

Our ARPES measurements have determined that the bands show minimal dispersion along the c-direction, thereby attesting to the quasi-two-dimensional nature of the bands. We have observed that there is a large discrepancy between the observed low-energy bands near the Γ point and the LSDA bands. The LSDA calculations show a 5f band that osculates the Fermi energy at the Γ point and disperses quadratically as k_x is increased. In addition, the LSDA calculations

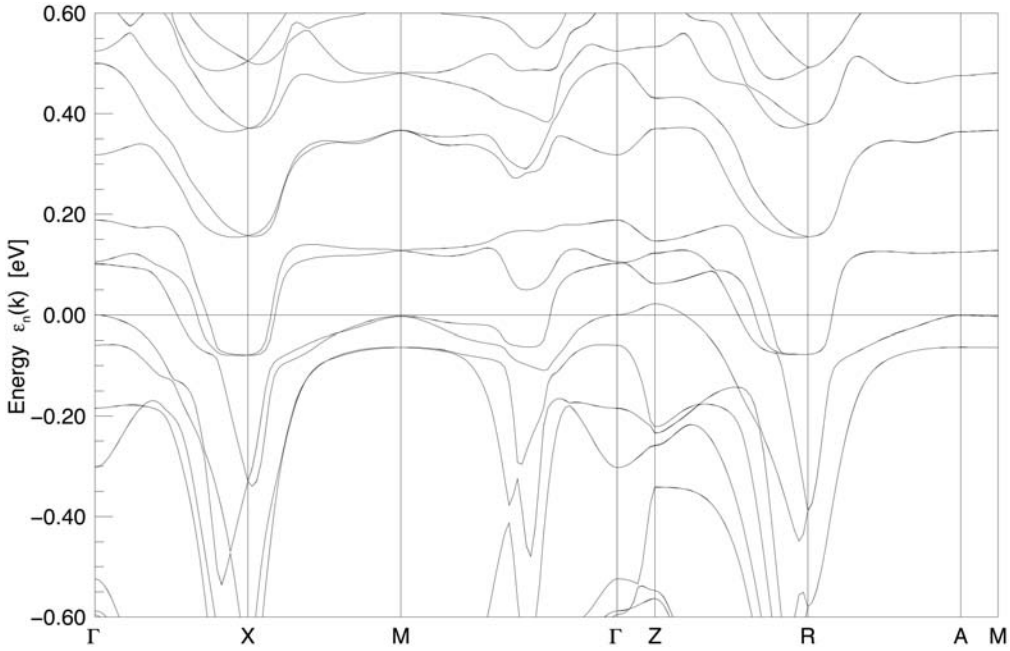

Figure 1. The LSDA bands near the Fermi energy for the antiferromagnetic phase of USb_2.

indicate that there is a second band at 110 meV above the Fermi energy which crosses the Fermi energy at

$$\left(\frac{k_F a}{\pi}\right) = 0.5455 \tag{1}$$

with a band mass of the same order of magnitude. Our ARPES results in the Γ-*X* direction are shown in Figure 2. It is seen that the spectrum at the Γ point is peaked about 17 meV below the Fermi energy, whereas the LSDA band touches the Fermi energy. As seen in panels (b) and (c) in Figure 3, the experimentally determined dispersion relation for this band is flatter than that found in the LSDA calculations and it exhibits a kink at an energy of about 21 meV which is attributed to a change in the quasiparticle mass by a factor of 2. Furthermore, the intrinsic width of the A peak near the Γ point is inferred to be extremely small, having a value of the order of 3 meV. The width of this peak remains small for small k_x values and increases rapidly for k_x larger than the kink. A kink in a quasiparticle dispersion relation that does not cross the Fermi energy is without precedent and does require a theoretical explanation. A fuller discussion of the experimental results is given below, and will be followed by a theoretical description. The paper will conclude with a comparison of experimental and theoretical results.

2. Experimental results

High-quality flux-grown single crystals were cleaved *in situ* in an ultra-high vacuum environment of less than 3×10^{-11} torr. A Neél temperature of 205 K was found from our

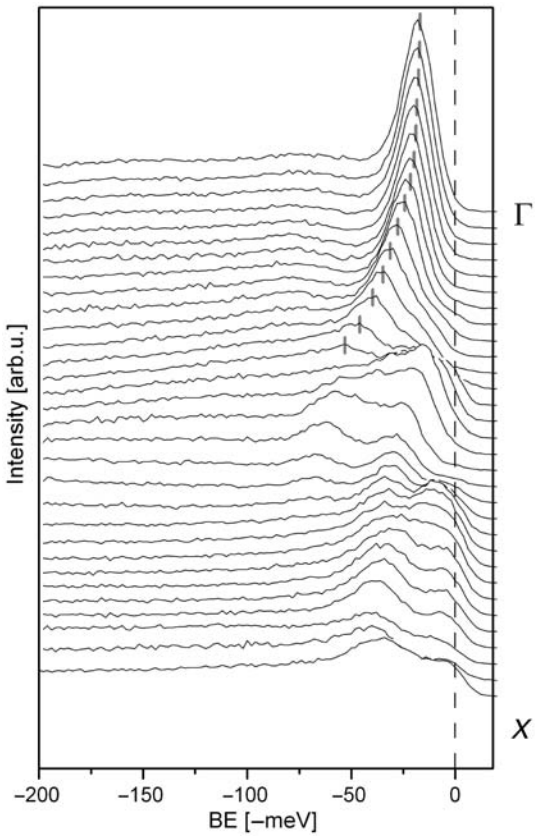

Figure 2. The ARPES spectra of USb_2 along the Γ-X direction. The vertical dashed line marks the position of the Fermi level.

susceptibility measurements. Prior to measurement, the crystal orientation was determined by X-ray diffraction. Angle-resolved photoemission was performed using the Plane Grating Monochromator beamline at the Synchrotron Radiation Center in Stoughton, Wisconsin. We used 34 eV photons, with an overall energy resolution better than 20 meV and an acceptance angle of ±1 degree. All measurements were performed at 15 K and the Fermi surface was referenced to the Fermi level of Pt. The spectral attributes of the quasiparticle peak were established by a nonlinear multiparameter regression fitting of the experimental data for each $\underline{k}$ value with a convolution of the Fermi function, a Gaussian with a width representing the energy resolution and an asymmetric Doniach–Sunjic (DS) with a width representing the intrinsic lifetime. The DS picture is implemented here simply to model the asymmetric variation in the Lorentzian component of the fit.

The electronic structure of USb_2 along the Γ-X direction is shown in Figure 2. Angular scans between the Γ and X points in the Brillouin zone of USb_2 are shown, where the photoemission intensity is normalized only by the photon beam intensity. The red markers indicate the quasiparticle peak binding energy obtained from a nonlinear fitting. The details of the electronic structure of USb_2 and a comparison with the LSDA calculation are presented in Figure 3. Here, panel (a) shows the energy distribution curve

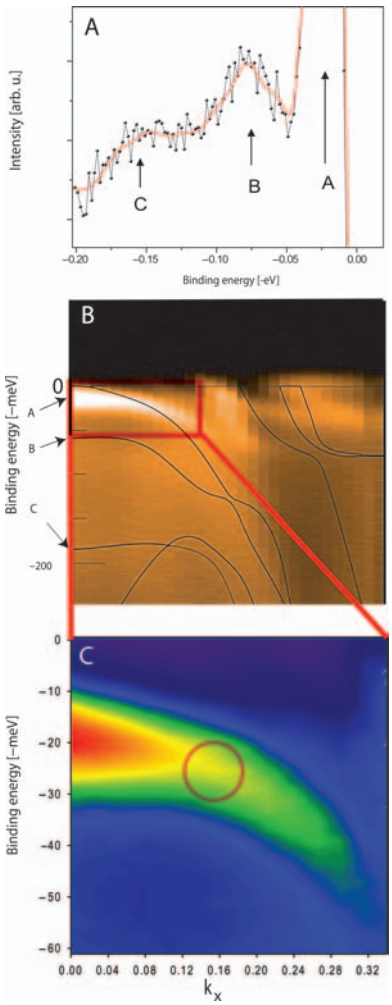

Figure 3. High-resolution angle-resolved photoemission spectra along the Γ-*X* direction. Panel (a) shows the energy distribution curve (EDC) in the vicinity of the Γ point. The characteristic features A, B and C are marked by arrows, and the red curve is a smoothed data line serving as a guide to the eye. In panel (b), the EDC intensities are shown together with the calculated LSDA dispersion relation. Panel (c) shows an expanded view of the marked subregion of (b), with a circle indicating the location of the kink.

(EDC) in the vicinity of the Γ point, with a scale designed to show the B and C bands clearly. The red line represents smoothed data as a guide to the eye. The bands A, B and C are marked with arrows. A contour plot of the EDC intensities between the Γ and X points
125 is shown in panel (b), and the characteristic features A, B and C are marked the same as in panel (a). The calculated LSDA band structure is also shown in panel (b) by black lines. Relatively good agreement is obtained between the energies of peaks B and C with the LSDA band energies at the high-symmetry point (Γ). However, as k_x is increased towards the X point, one can clearly notice discrepancies. In addition to being shifted away from

the Fermi energy, the measured band dispersion is flatter than in the LSDA calculations. The flattening of the band is restricted to energies within the first 20–50 meV below the Fermi level. Panel (c) shows the focus of our attention in this paper, namely an expanded view of the quasiparticle band A dispersing from the zone centre, with a clearly visible kink in the middle part of the panel.

Two distinct regions of the dispersion relation can be seen in Figure 3, which are separated by the kink. The k_x dependence of the peak binding energy and the peak width, respectively, are shown in panels (a) and (b) of Figure 4. Both the peak binding energy and the peak were found from a nonlinear multiparameter regression fitting of a single EDC scan for a given momentum value. If the measured band dispersion is denoted as $\epsilon_{\rm EXP}$, and the LSDA band dispersion $\epsilon_{\rm LSDA}$ is used as a bare band analogue, then a renormalization factor Z may be found by comparing the slope of $\epsilon_{\rm EXP} = Z^{-1}\,\epsilon_{\rm LSDA}$. In order to match the experimental dispersions, we have renormalized the original LSDA band curvature by the factor $Z_1^{-1} = 0.19$ in the binding energy (E_B) – momentum (k_x) space of ($-20 < E_B < 0, 0 < k_x < 0.18$), and by a factor of $Z_2^{-1} = 0.39$ in the region ($-60 < E_B < -20, 0.18 < k_x < 0.35$), where the energy is in units of meV and the momentum is in units of π/a. The kink appears near $E_B = -20$ meV and $k_x = 0.18$, as the separation of two distinct regions of the dispersion relation. The two distinct segments of the dispersion are shown in panel (a) of Figure 4 by the red and blue lines. The fits to the two segments of the dispersion relation are given by $\epsilon = -17.13 - 162.38\ k_x^2$ meV and $\epsilon = -12.77 - 331.03\ k_x^2$ meV for the red (Z_1) and blue (Z_2) parabolas, respectively. Hence, the effective quasiparticle masses m_1^* and m_2^*, for the Z_1 and Z_2 regions, respectively, are calculated from the curvatures, and the ratio m_1^*/m_2^* is found to be close to 2. The peak width is shown in panel (b) of Figure 4. It is seen that the peak width increases rapidly for k_x values larger than the kink position. From both panels, it can be seen that there is a distinct boundary between the two regions of k_x.

3. Theoretical model

The theoretical model assumes that the compensated metal has Fermi surfaces consisting of an f hole pocket and a conduction electron pocket with the same radii k_F, and that the light conduction electrons are responsible for the screening. We also assume a Debye spectrum for the acoustic phonons with a dispersion relation given by the expression

$$\omega_{\underline{q}} = c_L\ q \tag{2}$$

where the longitudinal speed c_L of sound is obtained from the Bohm–Staver model by

$$c_L^2 = \frac{4\ {Z_*}^2}{M\ k_F\ c}\left(\frac{\hbar^2\ \pi^2}{2\ m_e\ a^2}\right) \tag{3}$$

in which M is the mass of a uranium ion, $Z*$ is the ionic charge and (a, c) are the lattice parameters. In obtaining this approximate expression, we have noted that the c-lattice parameter is approximately twice the a-lattice parameter, and that there are two uranium atoms per unit cell. The electron–phonon interaction $\lambda_{\underline{q},\alpha}$ is given by [29]

$$\lambda_{\underline{q},\alpha} = i\left(\underline{q}\cdot\underline{\epsilon}_{\underline{q},\alpha}\right)\left(\frac{4\ \pi\ Z_*\ e^2}{\Omega_c\ (\ q^2 + q_{TF}^2)}\right)\sqrt{\frac{\hbar}{2\ M\ \omega_{\underline{q},\alpha}}} \tag{4}$$

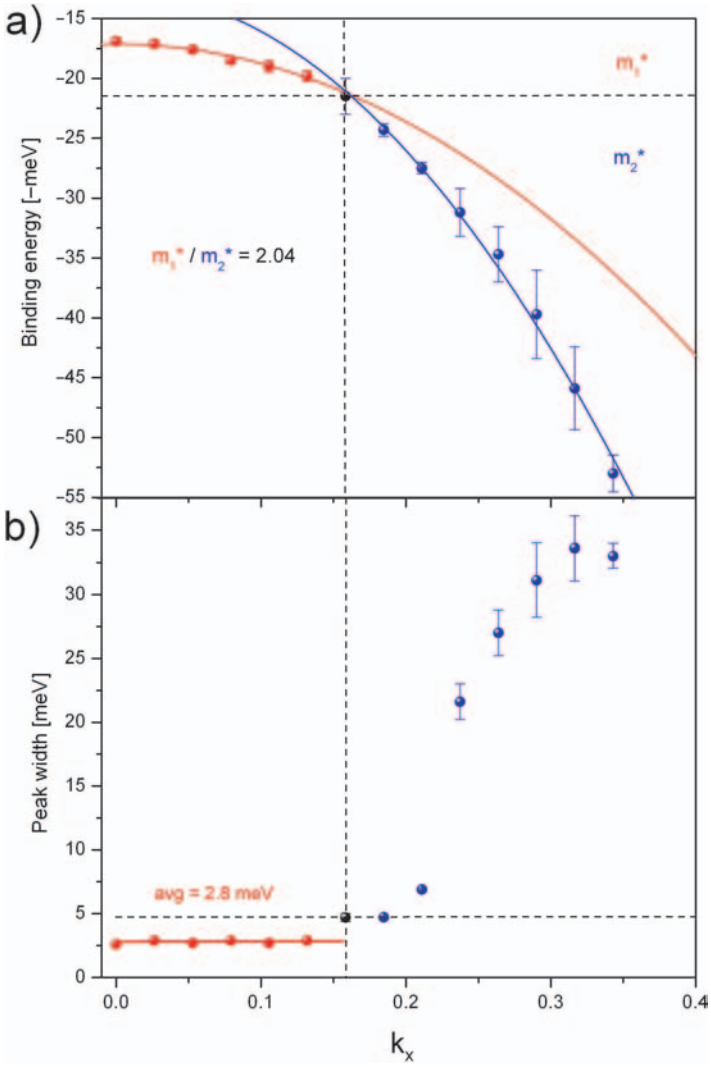

Figure 4. The energy of the spectral peak (a) and its width (b) for various k_x values.

where $\underline{\epsilon}_{q,\alpha}$ is the polarization vector and Ω_c is the volume per uranium ion

$$\Omega_c = \frac{1}{2}\, c\, a^2. \tag{5}$$

Due to the difficulty of obtaining analytic expressions for the interband matrix elements even in the short wavelength approximation [30,31], we shall simply scale the free-electron result according to the prescription

$$\lambda_{\underline{q},\alpha}^{\sigma,\tau} = \begin{pmatrix} \cos^2\Theta & \cos\Theta\sin\Theta \\ \sin\Theta\cos\Theta & \sin^2\Theta \end{pmatrix} \lambda_{\underline{q},\alpha} \tag{6}$$

where the mixing angle Θ is assumed to be independent of q (and k).

The dispersion relation for the two 5f bands under consideration are approximated by

$$\epsilon_k^{(1)} = -\frac{\hbar^2\ k^2}{2\ m_1} \tag{7}$$

and

$$\epsilon_k^{(2)} = \frac{\hbar^2}{2\ m_2}\ \left(\ k_F^2 - k^2\ \right). \tag{8}$$

As found in the LSDA calculation, the first band is below the Fermi energy but just touches the Fermi energy at $k=0$, whereas the second 5f band has a hole pocket of radius k_F. The relevant LSDA band masses are given by $m^{(1)} \approx 2.40\ \ m_e$ and $m^{(2)} \approx 5.53\ \ m_e$.

4. Calculation

The spectral density will be obtained by treating the electron–phonon interaction as a perturbation via Green's function techniques. The unperturbed single-electron Green's functions are denoted by $G_0^{\sigma,\tau}(k,\omega)$ and are given by

$$G_0^{\sigma,\tau}(\underline{k},\omega) = \frac{\delta^{\sigma,\tau}}{\hbar\omega + \mu - \epsilon_{\underline{k}}^{\sigma} + i\ \eta_{\underline{k}}} \tag{9}$$

where σ and τ are band indices. The Green's functions $G^{\sigma,\tau}(\underline{k},\omega)$ for the interacting electrons are given in terms of the bare Green's function and the self-energies $\Sigma^{\sigma,\rho}(\underline{k},\omega)$ via the matrix Dyson equations

$$G^{\sigma,\tau}(\underline{k},\omega) = G_0^{\sigma,\tau}(\underline{k},\omega) + \sum_{\rho,\lambda}\ G_0^{\sigma,\rho}(\underline{k},\omega)\ \Sigma^{\rho,\lambda}(\underline{k},\omega)\ G^{\lambda,\tau}(\underline{k},\omega). \tag{10}$$

Using the structure of the unperturbed Green's functions, Dyson's equations can be rewritten as a pair of matrix equations. One equations is given by

$$\begin{pmatrix} \hbar\omega + \mu - \epsilon_{\underline{k}}^{(1)} - \Sigma^{1,1}(\underline{k},\omega) & -\Sigma^{1,2}(\underline{k},\omega) \\ -\Sigma^{2,1}(\underline{k},\omega) & \hbar\omega + \mu - \epsilon_{\underline{k}}^{(2)} - \Sigma^{2,2}(\underline{k},\omega) \end{pmatrix} \begin{pmatrix} G^{1,1}(\underline{k},\omega) \\ G^{2,1}(\underline{k},\omega) \end{pmatrix} = \begin{pmatrix} 1 \\ 0 \end{pmatrix} \tag{11}$$

and the second matrix equation is obtained by interchanging the pair of indices $(1,2)$. Hence, one obtains the solutions as

$$G^{1,1}(\underline{k},\omega) = \frac{\hbar\omega + \mu - \epsilon_{\underline{k}}^{(2)} - \Sigma^{2,2}(\underline{k},\omega)}{(\ \hbar\omega + \mu - \epsilon_{\underline{k}}^{(1)} - \Sigma^{1,1}(\underline{k},\omega))\ (\ \hbar\omega + \mu - \epsilon_{\underline{k}}^{(2)} - \Sigma^{2,2}(\underline{k},\omega)) - \Sigma^{1,2}(\underline{k},\omega)\ \Sigma^{2,1}(\underline{k},\omega)} \tag{12}$$

and

$$G^{2,1}(\underline{k},\omega) = \frac{\Sigma^{2,1}(\underline{k},\omega)}{(\ \hbar\omega + \mu - \epsilon_{\underline{k}}^{(1)} - \Sigma^{1,1}(\underline{k},\omega))\ (\ \hbar\omega + \mu - \epsilon_{\underline{k}}^{(2)} - \Sigma^{2,2}(\underline{k},\omega)) - \Sigma^{1,2}(\underline{k},\omega)\ \Sigma^{2,1}(\underline{k},\omega)}. \tag{13}$$

The Green's functions $G^{2,2}(\underline{k},\omega)$ and $G^{1,2}(\underline{k},\omega)$ are given by similar expressions which are obtained by interchanging the indices $(1,2)$.

The matrix of electronic self-energies is calculated from the phonon emission and absorption processes [1,32] and is given by

$$\Sigma^{\sigma,\rho}(\underline{k},\omega)=\frac{1}{N}\sum_{\tau,\underline{q},\alpha}\lambda^{\sigma,\tau}_{\underline{q},\alpha}\;\lambda^{\tau,\rho\,*}_{\underline{q},\alpha}\left[\frac{1-f^{\tau}_{\underline{k}-\underline{q}}+N_{\underline{q}}}{\hbar\omega+\mu-\epsilon^{\tau}_{\underline{k}-\underline{q}}-\hbar\omega_{\underline{q},\alpha}}+\frac{f^{\tau}_{\underline{k}-\underline{q}}+N_{\underline{q}}}{\hbar\omega+\mu-\epsilon^{\tau}_{\underline{k}-\underline{q}}+\hbar\omega_{\underline{q},\alpha}}\right]. \tag{14}$$

The vertex corrections have been neglected in accordance with Migdal's theorem [33]. For the intraband scattering processes, the electron–phonon coupling constant will be assumed to be independent of the band indices σ and τ.

The ARPES spectrum for a band with index σ is denoted by the expression $A^{\sigma}(\underline{k},\omega)$ which is given by

$$A^{\sigma}(\underline{k},\omega)=-\frac{1}{\pi}\,\mathcal{I}m\;G^{\sigma,\sigma}(\underline{k},\omega). \tag{15}$$

In the next section, we shall examine the important contributions to the self-energy and describe their physical consequences. To clearly exhibit the origin of the kink in the osculating band, we shall also discuss the spectrum due to intraband processes in which the off-diagonal self-energies are artificially set to zero:

$$\Sigma^{\sigma,\tau}(\underline{k},\omega)=0\quad\text{for }\sigma\neq\tau. \tag{16}$$

In the approximation where the self-energy is diagonal in the band indices, the Green's functions simply reduce to the standard expression

$$G^{\sigma,\tau}(\underline{k},\omega)=\frac{\delta^{\sigma,\tau}}{\hbar\omega+\mu-\epsilon^{\sigma}_{\underline{k}}-\Sigma^{\sigma,\sigma}(\underline{k},\omega)}. \tag{17}$$

It will be seen that while the intraband processes do produce kinks in the dispersion relations of bands that cross the Fermi energy, intraband scattering processes do not yield kinks in bands that do not cross the Fermi energy. We shall then discuss the contribution to the interband self-energy which do produce the kink in the non-crossing band of USb_2.

4.1. *Intraband processes*

A. The kink in the crossing band

The self-energy due to intraband scattering processes gives rise to a kink in the dispersion of the second band, i.e. the band that crosses the Fermi energy. The forms of the real and imaginary parts of the self-energy are shown in Figure 5, for $k=k_F$ and $\Theta=\frac{\pi}{4}$. The self-energies are only slowly varying functions of k. It is seen that the real part of the self-energy varies linearly with ω in a frequency range of width $2\hbar\omega_D$ around the Fermi energy. This gives rise to a renormalization of the quasiparticle masses, through the mass enhancement factor Z_2 defined as

$$Z_2=1-\left.\frac{\partial\Sigma^{(2)}(k,\omega)}{\partial\hbar\omega}\right|_{\omega=0}. \tag{18}$$

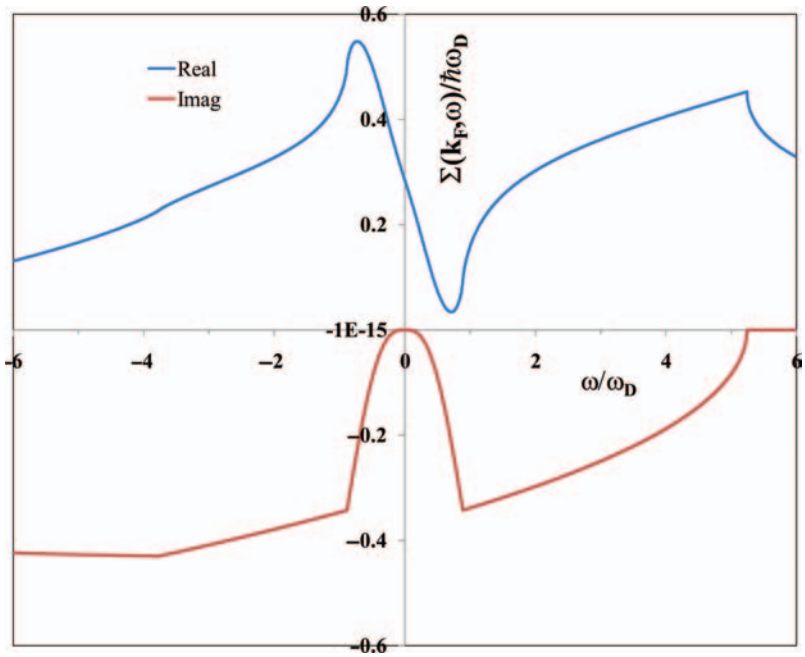

Figure 5. The real and the imaginary parts of the intraband self-energy $\Sigma^{(2)}(k_F, \omega)$ evaluated at the Fermi surface of the second band (in units of $\hbar\omega_D$), as a function of ω/ω_D.

The value of the real part of the self-energy at the Fermi energy $\omega = 0$ is a measure of the electron–hole asymmetry of the band, and is identically zero for a band with electron–hole asymmetry. This assertion concerning electron–hole symmetry is an immediate consequence of the imaginary part of the self-energy being an even function of ω due to electron–hole symmetry, which (through the Kramers–Kronig relation) leads to the real part of the self-energy becoming an odd function of ω. The imaginary part of the self-energy falls to zero at the Fermi energy, as is required for the quasiparticle concept to be valid, and has an envelope which is indicative of the density of states into which an electron or hole can be scattered. When only intraband processes are considered, the self-energy contributes a shift of the chemical potential given by

$$\mu = \epsilon^{(2)}_{k_F} + \Sigma^{(2)}(k_F, 0). \tag{19}$$

This shift is required by Luttinger's theorem [34] and by the conservation of electron number. As seen in Figure 6, at $k = k_F$ the spectrum for the second band shows a sharp delta function quasiparticle peak at the Fermi energy with weight Z_2^{-1} and two incoherent peaks with energies near $\pm\hbar\omega_D$ due to the emission and absorption of phonons. The intensity of the incoherent peaks can be seen to vanish almost linearly as $\omega \to 0$, which is a consequence of the approximate $\sqrt{q}$ variation of the electron–phonon coupling $\lambda_{q,\alpha}$ at small q. As k is changed slightly from below k_F to above k_F, the delta-function quasiparticle peak crosses the Fermi energy and there is a discontinuity in the occupied spectral weight n_k of magnitude Z_2^{-1}, instead of unity as is expected for non-interacting electrons [35]. It is seen that the discontinuity in n_k and the quasiparticle dispersion

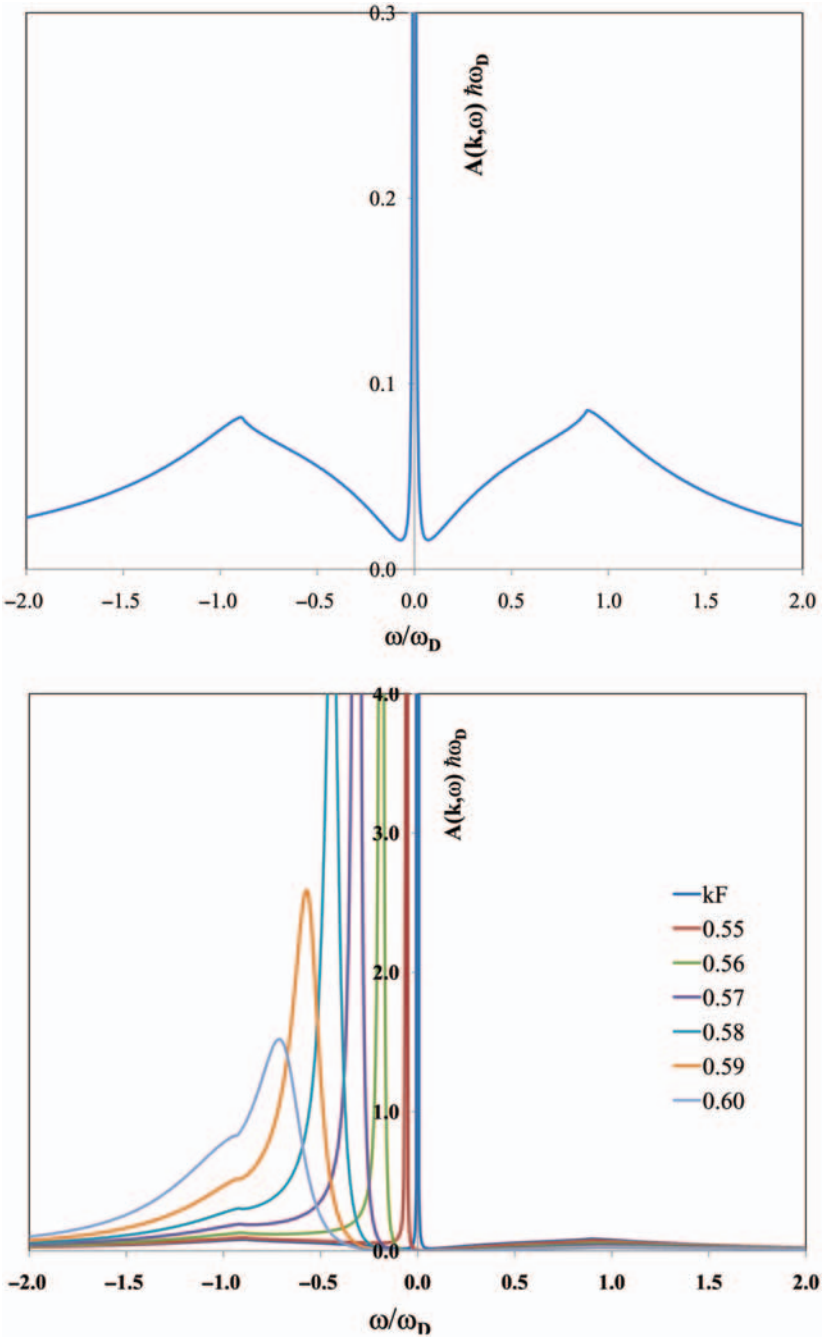

Figure 6. Top: The dimensionless spectral density $A^{(2)}(k_F, \omega)\ \hbar\omega_D$ evaluated at the Fermi surface, as a function of ω/ω_D. Bottom: $A^{(2)}(k, \omega)\ \hbar\omega_D$ versus ω/ω_D for the various values of (ka/π) shown in the legend.

relation are consistent with the value of $Z_2 = 1.37$. The difference between the interacting and non-interacting values of the jump is caused by the spectral weight in the incoherent portions of the spectrum, which reside both above and below the Fermi energy. It is also seen in the right panel that the quasiparticle delta function peak broadens and disperses as k moves off the Fermi surface. The energies of the peaks are shown in Figure 7 as a function of k. As is well known [1,32], the dispersion curve of the quasiparticle peak becomes flatter within $\pm\hbar\omega_D$ of the Fermi energy; the kink in the dispersion relation is due to the rapid increase in the quasiparticle mass due to the renormalization factor Z_2. For values of $\epsilon_k^{(2)}$ outside the window of $\pm\hbar\omega_D$ around the Fermi energy crossing, the mass renormalization is reduced to unity and the quasiparticle peaks broaden and become more symmetric, as seen by comparing Figure 8 with the right-hand panel of Figure 6.

B. The non-crossing band

By contrast, the intraband self-energy for a band which does not cross the Fermi energy, shown in Figure 9, has an imaginary part that falls to zero at an upper limit close to zero. The imaginary part of the self-energy falls to zero smoothly as $k \to 0$ since the phase space available for the emission of a phonon with wavevector q vanishes when $q \to 0$. Because of the smooth ω-variation of the imaginary part of the self-energy when $k \to 0$, the Kramers–Kronig relation produces a smoothly varying real part of the self-energy. Furthermore, since the band does not cross the Fermi energy, there is a maximal violation of electron–hole symmetry and the self-energy has a large value near the top of the band. Due to the smooth ω-variation of the real part of the self-energy, one finds that the intraband self-energy does not produce a significant contribution to the renormalization of the quasiparticle mass. Hence, one deduces that in the absence of interband transitions and when the band does not cut the Fermi energy, there is no kink in the quasiparticle dispersion relation. This is in accord with the experimentally determined valence bands of diamond which are in excellent agreement with the calculated tight-binding bands [36].

From the above discussions, the appearance of a kink in the dispersion relation and the absence of a decrease in the ω-integrated spectral weight on decreasing k, it is clear that the experimentally observed ARPES spectrum of USb_2 cannot described by only the intraband self-energy. It has to be investigated whether the interband processes are the origin of the downward shift and the kink in the osculating band. In the next subsection, we shall exhibit the properties of the dominant interband contribution to the self-energy $\Sigma^{1,1}(k, \omega)$.

4.2. *Interband processes*

The interband contribution to the self-energy $\Sigma^{11}(k, \omega)$ is primarily responsible for the large mass enhancement and the observed kink in the dispersion relation found in the non-crossing band in USb_2. The real and imaginary parts of the interband contribution to the self-energy are shown in Figure 10 for $k \approx 0$. It should be noted that since the low-energy behaviour of the interband self-energy is due to scattering from the state at $k = 0$ in the first band to states with $k \approx k_F$ in the second band, with either the emission or absorption of a phonon. Conservation of energy and momentum results in the imaginary part of the self-energy having a gap of width $\pm\hbar\omega_{k_F}$ centred on the Fermi energy. This gap is almost discontinuous, in contrast with the upper cut-off which is due to vertical interband

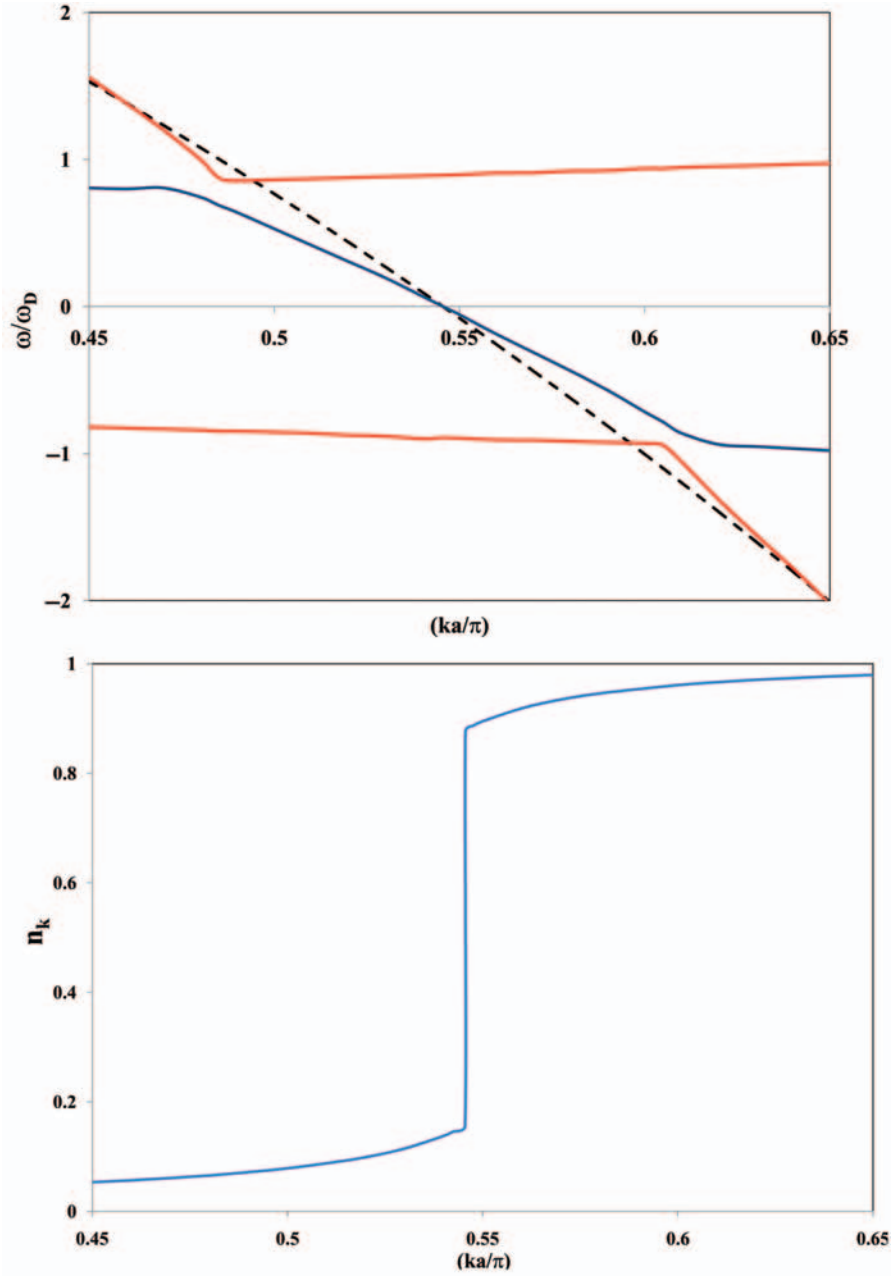

Figure 7. Top: The k-dependence of the energies of the features in $A^{(2)}(k,\omega)$. The bare band dispersion relation $\epsilon_k^{(2)}$ is depicted by the broken line. Bottom: The k-dependence of the occupation number n_k.

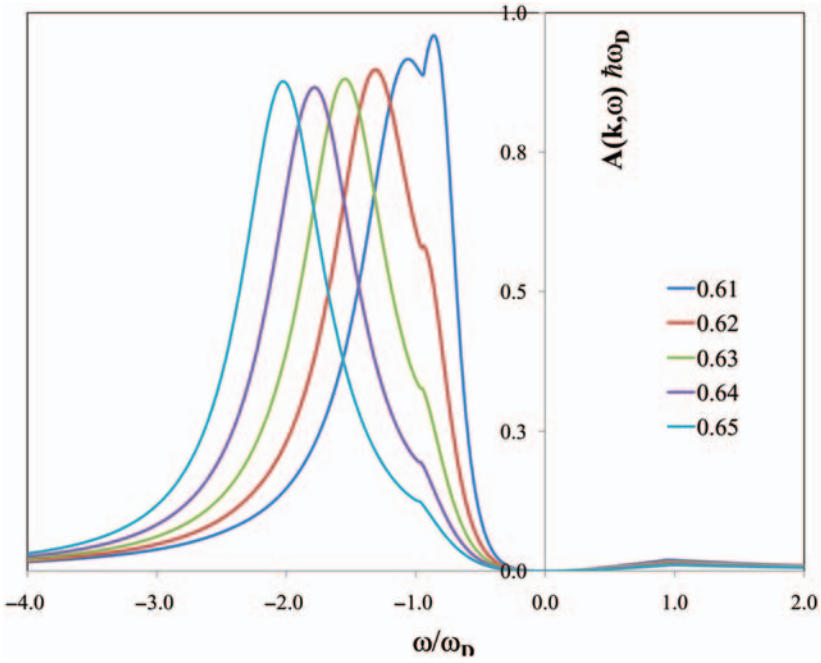

Figure 8. The dimensionless spectral density $A^{(2)}(k,\omega)\hbar\omega_D$ as a function of ω/ω_D, evaluated at various values of (ka/π) which are far removed from the Fermi surface.

transitions with zero momentum transfers ($q=0$). Due to the occurrence of the abrupt changes in the imaginary part of the self-energy, the real part of the self-energy exhibits logarithmic singularity-like variations at the gap edges. Furthermore, the derivative of the self-energy is large and negative in the region of the gap. On comparing the real part of this interband contribution to $\Sigma^{1,1}(k,\omega)$ with the intraband contribution to $\Sigma^{2,2}(k,\omega)$ one anticipates that, due to the closeness of the peaks and their increased strength, the non-crossing band might experience a larger mass enhancement than the crossing band. In the next section, we shall present the spectrum including all interband and intraband scattering processes.

5. Theoretical results

For the complete problem, when all the interband and intraband self-energies are included, the chemical potential is determined by the largest solution of the quadratic equation

$$(\mu - \epsilon^{(1)}_{k_F} - \Sigma^{1,1}(k_F,0))\,(\mu - \epsilon^{(2)}_{k_F} - \Sigma^{2,2}(k_F,0)) = \Sigma^{1,2}(k_F,0)\;\Sigma^{2,1}(k_F,0). \qquad (20)$$

The spectrum is given by Equation (15) and the Green's function diagonal in the band index is given by Equation (12). From Figure 11, it is seen that for small values of k the spectrum is mainly composed of a sharp peak at energies less than $\hbar\omega_{k_F}$. On increasing k, the peak rapidly broadens into an asymmetric peak as it enters the incoherent continuum. This rapid broadening is due to the existence of a threshold below which the large interband contribution to the imaginary part of the self-energy is located. As k is further

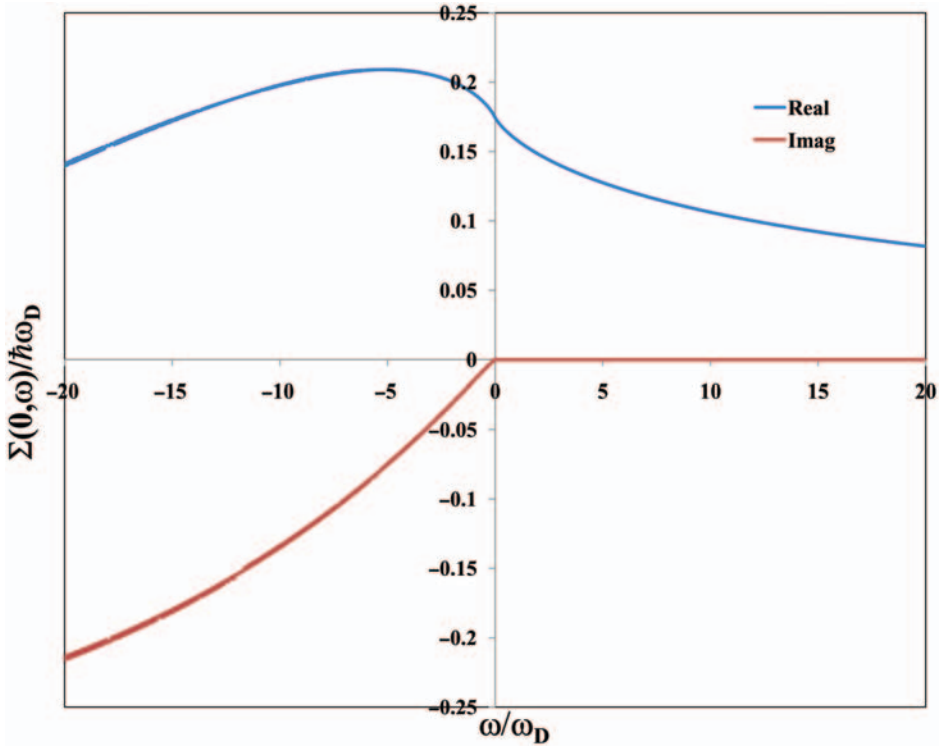

Figure 9. The real and the imaginary parts of the intraband self-energy $\Sigma^{(1)}(0,\omega)$ (in units of $\hbar\omega_D$) evaluated at the top of the non-crossing band, as a function of ω/ω_D.

increased, the main peak in the spectrum continues to gradually broaden and becomes more symmetric. The energy positions of the spectral features are shown in Figure 12. It is seen that the occupied portion of the spectrum for the non-crossing band has a finite threshold and has a kink in the dispersion relation which occurs at an energy of $\hbar\omega_{k_F}$. The energy of the kink in the non-crossing band is significantly smaller than the energy of the kink shown in Figure 7, which occurs at an energy $\pm\hbar\omega_D$. Also the mass renormalization factor associated with the non-crossing band has the value $Z_1 \approx 1.5$.

6. Conclusion

The experimental ARPES results on USb_2 show a band that has a maximum at 17 meV below the Fermi energy, but nevertheless shows a sharp cross-over between two distinct regimes of behaviour. At small k_x, the spectrum indicates that there is a branch of quasiparticles with renormalized masses and long lifetimes. For $k_x a/\pi$ values larger than about 0.18, the mass renormalization found from the quasiparticle dispersion relation drops by a factor of about 2 and the width of the spectrum rapidly increases. The cross-over between the two regions occurs at an energy of about 22 meV. This energy scale is significantly smaller than the Debye energy of 33 meV determined by Wawryk [20]. The theory shows that interband process can cause enhanced quasiparticles to exist in

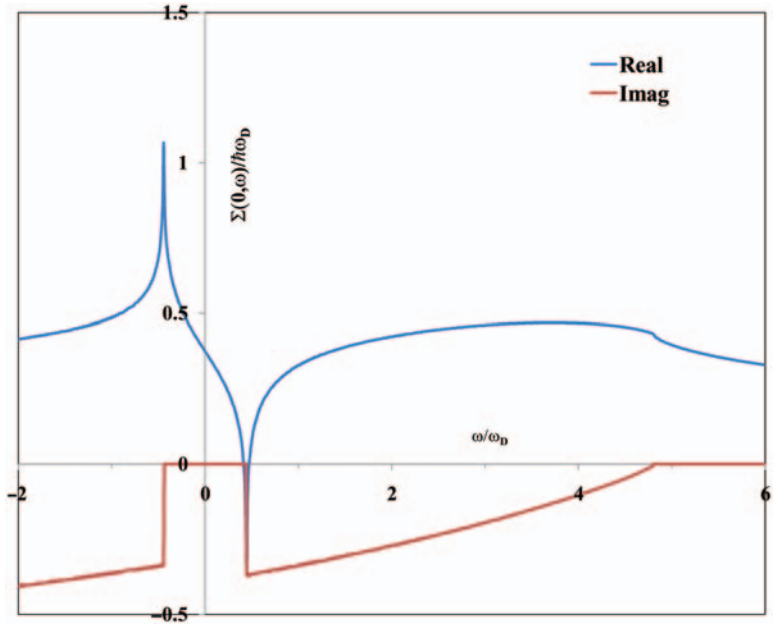

Figure 10. The real and imaginary parts of the interband contribution to the self-energy $\Sigma^{1,1}(0,\omega)$ in units of $\hbar\omega_D$ as a function of ω/ω_D.

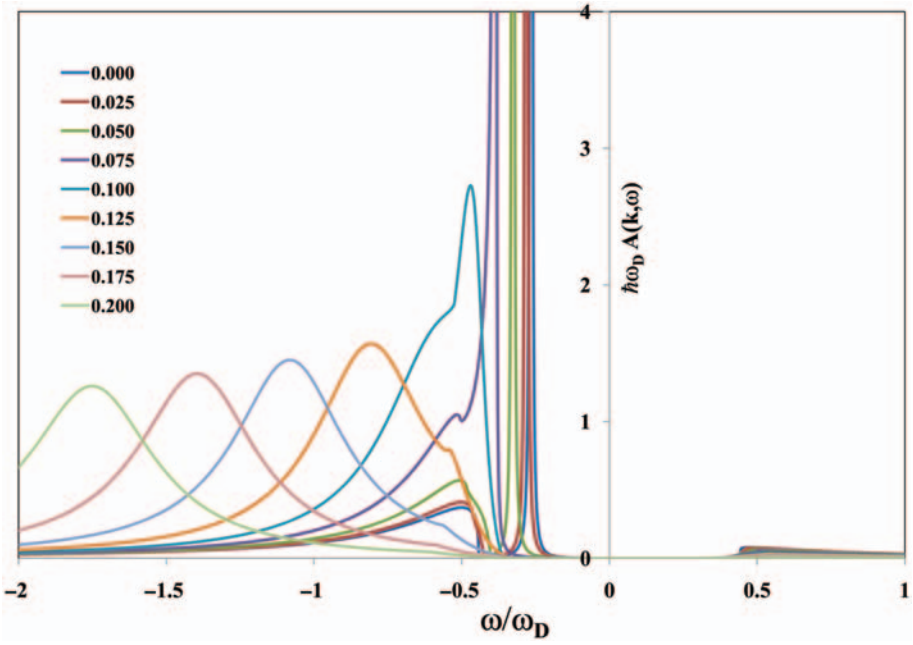

Figure 11. The spectral density of the non-crossing band $\hbar\omega_D\ A^{(1)}(k,\omega)$ as a function of ω/ω_D, for the various values of ka/π shown in the legend. The calculation corresponds to the value of $\Theta = 0.966$.

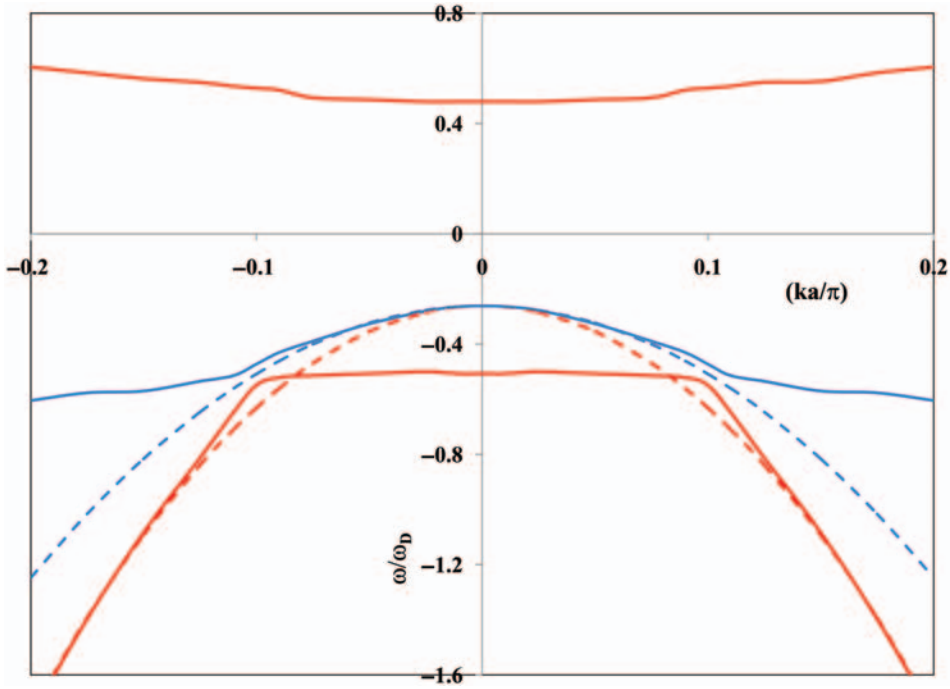

Figure 12. The energies of the features in the spectra of the non-crossing band $A^{(1)}(k,\omega)$ as a function of ka/π. The dashed red line is the (rigidly shifted) LSDA dispersion relation. The dashed blue line represents the (rigidly shifted) LSDA dispersion relation modified by a mass renormalization factor of $Z_1 = 1.5$.

bands that reside totally below the Fermi energy, and that these quasiparticle bands undergo a cross-over to unrenormalized bands with large scattering rates. The cross-over occurs at quasiparticle energies of the order of $\hbar\omega_{k_F}$, which are estimated to occur at about $0.5\ \hbar\omega_D$ and $ka/\pi \approx 0.1$ instead of the value of 0.18 deduced from experiment. While this can be considered as being in reasonable agreement, specially with consideration of the crudeness of the three-dimensional theoretical model, there do still exist significant discrepancies. Namely, the experimentally determined bands do not collapse onto the unrenormalized LSDA bands when they are below $\hbar\omega_{k_F}$ of the Fermi energy (even if the LSDA bands are shifted relative to the Fermi energy). This failure is indicative of the presence of another source of mass renormalization and another energy scale, which is probably due to antiferromagnetic spin fluctuations.

Acknowledgements

The authors would like to thank James L. Smith for his friendship, support and encouragement over the years. The work at Temple University was supported by the US Department of Energy, Office of Basic Energy Sciences. Work at LANL was performed under the auspices of the US DOE and LANL LDRD Program. The SRC is supported by the NSF under Award Np. DMR-0084402. Support from the Swedish Research Council (VR), SNIC, and European Commission (JRC-ITU) is gratefully acknowledged. EG was supported by Polish grant N202 140 32/3877. Thanks are due to

K. Byczuk, A. Kaminski, J.D. Thompson, F. Ronning, T. Klimczuk, C. Batista, A. Balatsky and Y.-F. Yang for stimulating discussions.

References

[1] S. Engelsberg and J.R. Schrieffer, Phys. Rev 131 (1963) p.993.
[2] S. Doniach and S. Engelsberg, Phys. Rev. Lett 17 (1966) p.750.
[3] N.F. Berk and J.R. Schrieffer, Phys. Rev. Lett 17 (1966) p.433.
[4] W.F. Brinkman and S. Engelsberg, Phys. Rev 169 (1968) p.417.
[5] P.S. Riseborough, Phil. Mag. 86 (2006) p.2581.
[6] T. Moriya and A. Kawabata, J. Phys. Soc. Japan 34 (1973) p.639.
[7] T. Moriya and A. Kawabata, J. Phys. Soc. Japan 35 (1973) p.669.
[8] K. Byczuk, M. Kollar, K. Held et al., Nature Phys 3 (2007) p.168.
[9] A. Lanzara, P.V. Bogdanov, X.J. Zhou et al., Nature 412 (2001) p.510.
[10] Z.-X. Shen, A. Lanzara, S. Ishihara et al., Phil. Mag. B 82 (2002) p.1349.
[11] P.D. Johnson, T. Valla, A.V. Fedorov et al., Phys. Rev. Lett. 87 (2001) p.177077.
[12] A. Kaminski, M. Randeria, J.C. Campuzano et al., Phys. Rev. Lett. 86 (2001) p.1070.
[13] G.R. Stewart, Z. Fisk, J.O. Willis et al., Phys. Rev. Lett. 52 (1984) p.679.
[14] L. Taillefer, R. Newbury, G.G. Lonzarich et al., J. Mag. Mag. Mat. 63-64 (1987) p.372.
[15] N. Kimura, T. Komatsubara, D. Aoki et al., J. Phys. Soc. Japan 67 (1998) p.2185.
[16] P.S. Riseborough, Phys. Stat. Sol. B 122 (1984) p.161.
[17] S. Donovan, A. Schwartz and G. Grüner, Phys. Rev. Lett. 79 (1997) p.1401.
[18] F. Grønvold, M.R. Zaki, E.F. Westrum Jr et al., J. Inorg. Nucl. Chem. 40 (1978) p.635.
[19] J. Leciejewicz, R. Troc̀, A. Murasik et al., Phys. Stat. Sol. 22 (1967) p.517.
[20] R. Wawryk, Phil. Mag. 86 (2006) p.1775.
[21] Z. Henkie and Z. Kletowski, Acta Phys. Pol A 42 (1972) p.405.
[22] D. Aoki, P. Wisniewski, K. Miyake et al., Phil. Mag. B 80 (2000) p.1517.
[23] P. Wisniewski, P.D. Aoki, N. Watanabe et al., J. Phys. Soc. Japan 70 (2001) p.278.
[24] D. Aoki, P. Wisniewski, K. Miyake et al., Physica B: Cond. Mat. 281 (2000) p.761.
[25] D. Aoki, P. Wisniewski, K. Miyake et al., J. Phys. Soc. Japan 68 (1999) p.2182.
[26] S. Lebègue, P.M. Oppeneer and O. Eriksson, Phys. Rev. B 73 (2006) p.045119.
[27] K. Koepernik and H. Eschrig, Phys. Rev. B 59 (1999) p.1743.
[28] J.P. Perdew and Y. Wang, Phys. Rev. B 45 (1992) p.13244.
[29] F. Bloch, Z. Physik 52 (1928) p.580.
[30] L.-J. Sham, Proc. Phys. Soc. London 78 (1961) p.895.
[31] R.T. Shuey, Phys. Rev. A 139 (1965) p.1675.
[32] D.J. Scalapino, J.R. Schrieffer and J.W. Wilkins, Phys. Rev. 148 (1966) p.263.
[33] A.B. Migdal, Sov. Phys. JETP 7 (1958) p.996.
[34] J.M. Luttinger, Phys. Rev. 119 (1960) p.1153.
[35] A.B. Migdal, Sov. Phys. JETP 5 (1957) p.333.
[36] I. Jimènez, L.J. Terminello, D.G. Sutherland et al., Phys. Rev. B 56 (1997) p.7215.